TOPICAL REVIEW

Recent advances in 3D porous MXenes: structures, properties and applications

To cite this article: Qiuyang Yan *et al* 2022 *J. Phys. D: Appl. Phys.* **55** 093001

IOP Publishing Journal of Physics D: Applied Physics
J. Phys. D: Appl. Phys. **55** (2022) 093001 (15pp) https://doi.org/10.1088/1361-6463/ac2db2

Topical Review

Recent advances in 3D porous MXenes: structures, properties and applications

Qiuyang Yan[1,2], Yin Cheng[1,*], Ranran Wang[1,3,*] and Jing Sun[1]

[1] State Key Laboratory of High Performance Ceramics and Superfine Microstructure Shanghai Institute of Ceramics Chinese Academy of Science, Shanghai 200050, People's Republic of China
[2] University of Chinese Academy of Sciences, Beijing 100049, People's Republic of China
[3] School of Chemistry and Materials Science, Hangzhou Institute for Advanced Study, University of Chinese Academy of Sciences, Hangzhou 310024, People's Republic of China

E-mail: chengyin.1989@qq.com and wangranran@mail.sic.ac.cn

Received 1 July 2021, revised 31 August 2021
Accepted for publication 7 October 2021
Published 28 October 2021

Abstract

3D porous MXenes have recently attracted great attention as they possess appealing electrical and mechanical properties, which enable their excellent performance in expanding application scopes like electromagnetic interference shielding, energy conversion and storage, and smart sensing. New methods have been developed for their synthesis and 3D porous structure design, as well as the tuning of properties for practical applications. Nevertheless, the fundamental understanding of their structure–property relationships remains obscure, hindering the further exploitation of their untapped potential in myriad applications. In this review, recent studies of porous MXenes are discussed regarding their synthesis, structure, properties, and applications. We also elaborate on the possible correlation between structure and properties through a comprehensive comparison of typical porous MXene examples. Finally, the challenges and perspectives for advancing the study and applications of porous MXenes are presented.

Keywords: 3D porous MXenes, EMI, energy conversion and storage, smart sensing

(Some figures may appear in colour only in the online journal)

1. Introduction

MXene, a new family of two-dimensional (2D) materials, has attracted considerable attention since it was first synthesized by Yury Gogotsi in 2011 [1]. Generally, MXene is prepared by etching the A layer in the MAX precursors (M denotes the transition metals, A is for the elements in group IIIA or IVA, and X is carbon and/or nitrogen). Due to their superior conductivity and mechanical properties, MXenes are well-suited for multiple application fields, such as energy conversion and storage [2–11], electromagnetic interference (EMI) shielding [12–26], and sensors [27–34]. Considering the rich diversity in etching (such as HF (hydrofluoric acid) etching and mild LiF/HCl etching) and delamination (sonication, TMAOH intercalation, etc) methods, it is feasible to adjust the morphology and the termination of the MXe surface for specific targeting applications. In addition, various micro- and macrostructures of the MXenes have been explored to broaden their EMI/sensing range. In contrast to compacted films and fibers, the 3D porous MXenes allow abundant space for structure adjustment, including porous films with macro pores [9, 17, 20, 35–38], aerogels [4, 7, 15, 23, 27–29, 31, 39–47], hydrogels [5, 48–51] and sponges [12, 52–54]. For instance, MXene films with macro pores could be prepared by foaming with hydrazine after filtration [3, 11, 17], exhibiting better EMI shielding performance (SE) than those normal films without foaming treatment. In addition, MXene aerogels fabricated by freeze-drying perform excellently when applied to

* Authors to whom any correspondence should be addressed.

batteries and super capacitors (SCs). MXene-based sponges also show high sensitivity when utilized as sensors. However, the relationship between the structure and performance is still not clear. This impedes the development of judicious and efficient design guidelines for porous MXenes with customized performance.

Several reviews [55, 56] about 3D porous MXenes have been published so far. However, few of them pay attention to the structure–property relationship of porous MXenes, which is crucial for the purposeful design of materials. This review comprehensively introduces the latest progress in fabrication, property, and application of porous MXenes. First, porous MXenes are classified into three categories according to the fabrication methodology and corresponding distinct structures. Second, the inter-relationship between the preparation, structure, and property is revealed by elaborating on a few representative examples regarding their structure design and performance optimization. Third, we discuss the prevalent applications of porous MXenes. Finally, the current challenges and prospects of porous MXenes are presented.

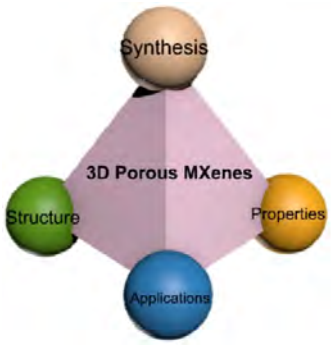

2. Preparation and structures of porous MXenes

A variety of fabrication methods for porous MXenes have been reported in the past few years, and there are three main categories: foaming, cross-linking, and templating. The preparation method plays a decisive role in defining the overall porous structure of MXenes and the processing condition ensemble can finely tune the structural parameters like pore volume and wall thickness. In this section, we discuss recent studies on the preparation and structural design avenues of porous MXenes.

2.1. Foaming method

The form factor of film structure is in demand for many practical applications, and is easy to deploy in various environments. However, re-stacking is inevitable due to strong van der Waals forces between the 2D nanosheets, resulting in high density, low porosity, hydrophilicity and other unfavorable properties. A rational strategy to address this issue is foaming the film by hydrazine treatment after filtration [3, 11, 17]. In this way, a 3D film-like porous MXene can be prepared with considerably decreased density, largely extended surface area, hydrophobicity, and numerous active sites.

As observed in many studies, the 2D MXene nanosheets are well-aligned with stacking during filtration and then an ordered, compact, and lamellar structure is formed. The hydrophilic nature of MXene and the considerable tiny pores between the layers collaboratively allow the access of hydrazine molecules into the interlamination of the MXene films, therefore expanding the interlayer space and inducing the formation of porous MXenes. In 2017, Zhang's group [17] fabricated 3D porous MXene film by foaming method as illustrated in figure 1(A). First, they prepared MXene films by vacuum filtration, which were then sandwiched between two ceramic wafers and coated with hydrazine monohydrate (80%), followed by thermal treatment at 90 °C for a certain time. In this process, the rapid evaporation of the hydrazine infiltrated into the film induces the production of extensive interconnected pores, thus expanding the film. It is worth noting that the foam thickness is related to the mass of the infiltrated MXene [17], which means that they can tune its thickness according to the requirement of the real application conveniently. In addition, the amount of the added hydrazine monohydrate plays an essential role in the expansion of the MXene films. Briefly, the more the hydrazine is added, the larger the thickness increases [11]. As depicted in figure 3(G), the obtained MXene foams show an obvious volume expansion and have a loose cellular structure, providing intensive active sites and large surface area.

2.2. Cross-linking method

The conventional approach to fabricating porous aerogels consists of three steps: (a) preparation of uniformly dispersed precursor solutions; (b) gelation process; and (c) drying treatment. The gelation process has a direct influence on the final structure of the aerogel. However, it is difficult to achieve gelation of MXene sheets due to their strong hydrophilicity. The small contact angle caused by abundant surface functional groups makes MXene tend to get evenly dispersed in the solution rather than be assembled. Great efforts have been devoted to achieve the gelation process by means of destroying the charge balance in the solution. The most widely used method is to introduce metal ions or cross-linkers with different charges or zeta potentials into the MXene solution system, providing strong electrostatic adsorption against the exclusive force between the nanosheets. Relevant fabrication processes of porous MXenes with different types of cross-linkers have been shown in figures 1(B)–(E). In addition, considering that the network of gels tends to collapse due to the large capillary force during the drying process, freeze-drying is applied to retain the framework of MXene hydrogels.

Graphene oxide (GO) is a typical choice as a cross-linker because of its excellent gelation ability [8, 15, 41, 57, 58]. In 2019, Huang's group fabricated MXene/GO aerogel by cross-linking method as shown in figure 1(B). First, they formed a homogeneous MXene/GO solution with a certain ratio. After hydrothermal treatment, partial GO was reduced to reduced graphene oxide (rGO) and therefore the zeta potential was increased, thus decreasing the electrostatic repulsion and making gelation possible. In this process, self-assembly

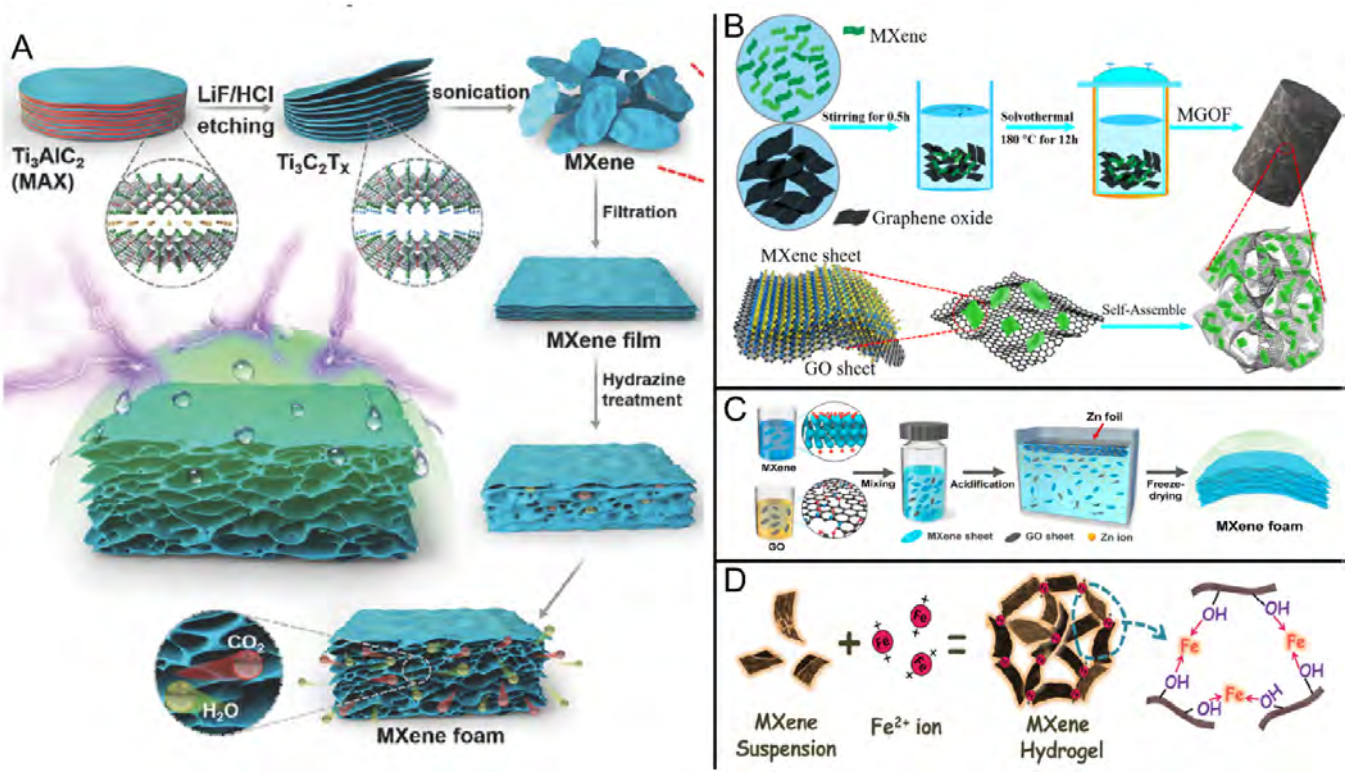

Figure 1. Schematic illustration of various fabrication processes of porous MXenes. (A) Foaming method [17]; reproduced with permission. Copyright 2017, Wiley. (B) Cross-linking method (with assistant of GO) [41]; reproduced with permission. Copyright 2019, American Chemical Society. (C) Cross-linking method (with assistant of GO and Zn foils) [16]; reproduced with permission. Copyright 2020, American Chemical Society. (D) Cross-linking method (with assistant of metal ions) [5]; reproduced with permission. Copyright 2019, Wiley.

occurred in the solution and a hydrogel could be obtained, which was then freeze-dried to get the final aerogel. Generally, the reduction process could also be achieved by adding reductants such as HI [57] and vitamin C [58]. The addition of a reducing agent can not only reduce the GO but also prevent the oxidation of MXene. Temperature and heating time should be adjusted when using different reductants. As mentioned above, the assembly capability mainly comes from the GO and rGO. The GO/rGO forms the supporting porous skeleton as the framework, upon which the MXene sheets are uniformly distributed. Thus, it is not surprising to find that the structure of the hybrid MXene/rGO aerogel is similar to that of the rGO aerogel [27, 57, 58]. Nevertheless, the large size difference between the MXene and rGO influences their specific structural parameters, which means that the ratio of MXene to rGO should be noticed according to the application requirements [59].

The self-assembly of MXene/GO could be achieved with the assistance of metal ions without thermal treatment [16, 60–62]. Tan's group [16] fabricated hybrid foams by utilizing Zn foils as an ion-supply and absorber. Initially, they mixed the MXene and GO suspension with acidification of HCl. The mixed suspension was then kept standing with a cleaned Zn foil immersed for a certain time, during which the metal would be oxidized and release electrons, destroying the electrostatic balance and reducing the GO nanosheets. Therefore, the MXene/GO with negative zeta potential tended to aggregate near the left positively charged metal foil surface, making gelation possible. After detaching and dialysis, a hydrogel was obtained with lamellar structure (figure 3(B)), and freeze-drying was conducted to get the required aerogel. Similar reactions took place with other metal foils (Al, Co, Ni, Fe, etc) and the pore size and thickness of the aerogel could be tuned by adjusting the acidification degree (pH) and gelation time. In addition, Yang's group [5] utilized the metal ions directly to assist the gelation of MXene nanosheets without GO and obtained a porous MXene hydrogel as shown in figure 1(D). They found that the concentration of the MXene solution and the mass ratio of the metal ion to MXene both show profound impacts on the structure of the hydrogels. Interestingly, the ions with two positive charges show the best gelation effect.

Additionally, cross-linking can be realized with the assistant of ethylenediamine (EDA) [48, 63], epichlorohydrin (ECH) [64], and ammonia [65]. Due to the abundance of hydroxyl groups on the MXene surface, it is easy for these cross-linking agents to build covalent bonds on MXene sheets with grafting reactions. Hydrogen-bond interactions also play an important role in the gelation of the MXene suspension. Sui's group [64] fabricated directional porous structure with the aid of ECH. First, micro-crystalline cellulose, ECH and MXene powders with different ratios were mixed into prepared aqueous alkali hydroxide/urea solution, followed by sonication and stirring. The resulting suspension

was then gelled at room temperature due to the ECH-enabled bonding of the MXene sheets and cellulose. Residual alkali hydroxide/urea components and water molecules were removed by washing and freeze-drying. Interestingly, a structure with lamellar channels distributed throughout the aerogel was created, which is different from the typical structure of MXene hydrogels. This difference may be caused by the growth of ice crystals during the freezing process, which breaks the walls perpendicular to the direction of ice growth.

2.3. Templating method

The templating method is the most widely used method in the preparation of porous MXenes, especially porous MXenes with their unique structure and special properties. In this way, the materials and structures of the template can be designed according to the required performance to meet individual requirements in practical applications. Generally, the templating method can be classified into the following categories based on the type of templates: direct absorption method, sacrificial template method, emulsification method, and ice template method. The structure of porous MXenes varies with the method and fabrication conditions.

2.3.1. Direct absorption method. The direct absorption method is one of the most convenient approaches to building porous MXenes and the structure of templates can be retained well in the resulting samples. Ni foam (NF) [2, 66–68], polyurethane foam (PUF) [69, 70], melamine foam (MF) [12, 71] and carbon foam (CF) [19] are common templates with excellent hydrophilicity. Generally, templates with porous structure are immersed into an assistant solution (polyvinyl alcohol (PVA), chitosan solution or others) and MXene solution repeatedly, as shown in figure 2(A). MXene sheets adsorb on the surface of the templates during the dip-coating process. After layer-by-layer deposition, the obtained sample can be dried at room temperature or freeze-dried. The structures of porous MXenes prepared by these means are similar due to the confinement of the templates as depicted in figure 3(G). The pore size is of the order of hundreds of microns for PUF and NF, and dozens of microns for MF and CF, respectively.

2.3.2. Sacrificial template method. Templates can serve as skeletons to support MXene sheets as introduced above. Nevertheless, the hydrophilicity of the templates limits the absorption of the MXene solution. Meanwhile, the existence of templates is adverse to the pursuit of high electrical conductivity and low density of porous MXenes. Sacrificial template methods are regarded as a helpful way to diversify the structure of porous MXenes and improve their properties. NFs [75], porous MXene spheres [20, 73] and sulfur [6] are attractive templates, which can be removed after the formation of 3D porous networks. Yu's group [75] fabricated MXene/NF hybrid foam by means of direct absorption, followed by polydimethylsiloxane (PDMS) infiltration and etching of NF. An MXene/PDMS composite with an inverted structure of NF was finally obtained. Besides, Gogotsi's group [73] constructed a 3D macro-porous MXene framework by filtration of the mixture of MXene solution and porous MXene sphere dispersion and subsequent annealing treatment with argon protection. Porous MXene spheres in the filtrated film were removed at high temperature, leaving film-like porous MXenes with spherical porous macrostructure (figure 2(C)). The pore size could be tuned by modulating the size of porous MXene spheres, which showed an important influence on the properties of the porous MXenes. In addition, sulfur can be employed similarly as porous MXene spheres to generate sphere pores [6].

2.3.3. Emulsification method. The emulsification method employs oil and water as templates to prepare porous MXenes. Severe shaking would emulsify the solution, and the MXene sheets could be trapped at the oil/water interface due to the amphipathic feature of the treated MXene sheets, forming a porous structure after the removal of the oil/water. In 2018, Huang's group [76] studied the modification of MXene sheets surface assisted by cetyltrimethylammonium bromide (CTAB) to adjust their hydrophilic–hydrophobic balance and fabricated porous MXenes by the emulsification method. First, CTAB solution was added into the MXene suspension with different pH, which was tuned by the addition of HCl or NaOH solution. The CTAB loaded on the surface of the MXene sheets could make it partially wet, satisfying the requirement of the subsequent dodecane droplets stabilizing. The solution was then vortex-mixed with dodecane, forming the Pickering emulsions. After that, the 2-hydroxyethyl methacrylate and the initiator azodiisobutyronitrile were added into the solution with a certain ratio to achieve polymerization, and then drying treatment was applied to obtain the porous MXenes. Within a neutral or alkaline environment, stable emulsions can be achieved without phase separation, allowing the formation of 3D porous structures. Later, Zhang's group [72] prepared porous MXenes with sphere-like porous structure as illustrated in figure 2(B). First, they mixed MXene suspension and POSS-NH_2 solution (oil-soluble amine-functionalized polyhedral oligomeric silsesquioxane) with a determined ratio. After shaking the mixture, MXene sheets were surface activated, and a stable emulsion was achieved with MXenes assembled at the oil/water interface. Subsequently, a dense cream was collected via centrifugation treatment and then freeze-dried to remove the residual water and oil. As figure 3(A) shows, the pore size and shape of the porous MXene is inherited from the emulsion droplets.

2.3.4. Ice template method. Water is readily available in the laboratory and the hydrophilicity of MXene sheets makes ice template methods easy to conduct. During the freezing process, the MXene would be repelled from the solid/liquid interface and entrapped within the ice crystals, resulting in the formation of porous MXenes [4, 7, 9, 10, 22, 25, 27, 33, 42, 43, 46, 74, 77–84]. The factors of the precursor solution (such as concentration, pH, viscosity, etc) and temperature condition have a crucial influence on the

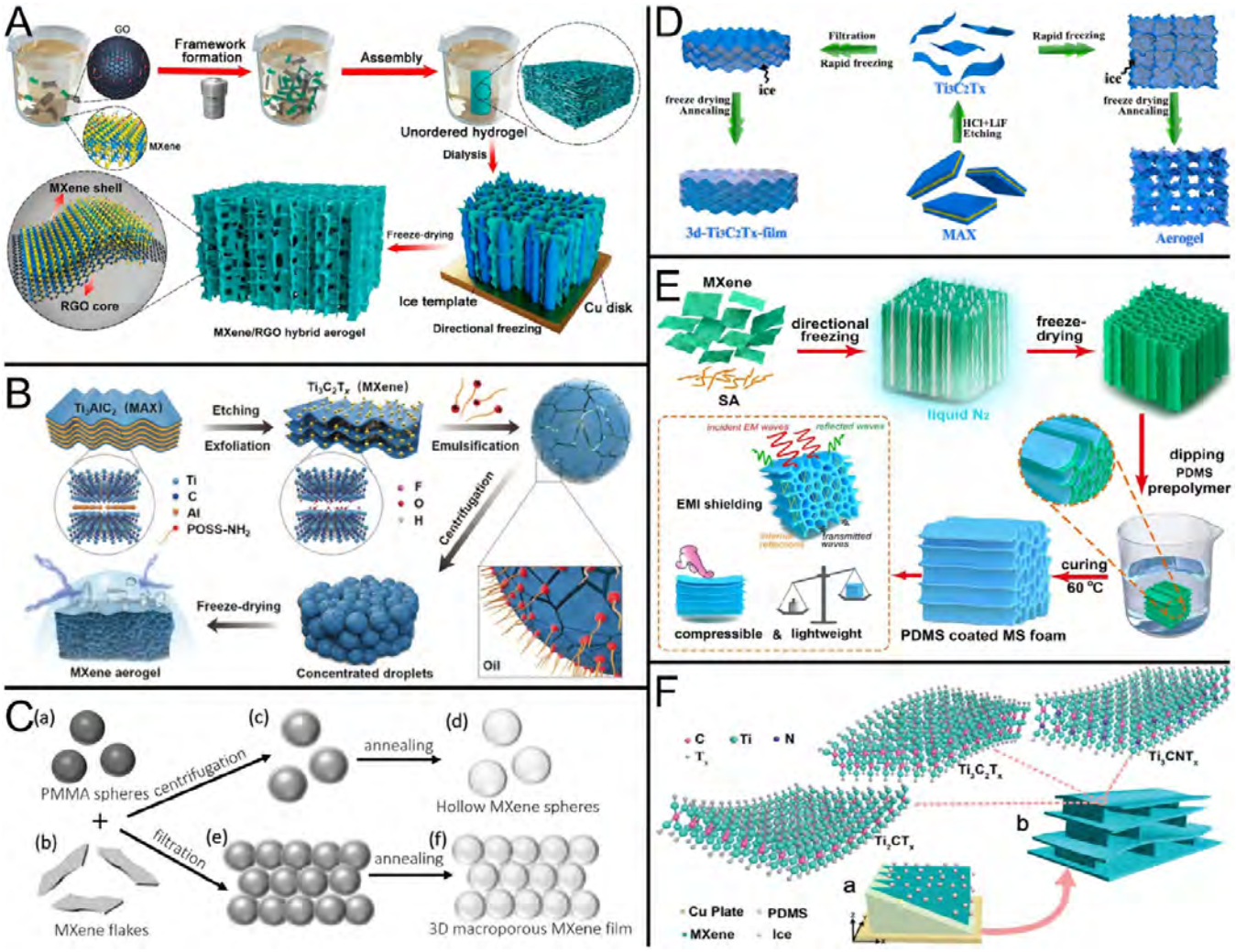

Figure 2. Schematic illustration of various fabrication process of the porous MXenes by various methods. (A) Cross-linking method (with assistance of GO) [15]; reproduced with permission. Copyright 2018, American Chemical Society. (B) Emulsification method [72] (with assistance of CTAB activated); reproduced with permission. Copyright 2019, Wiley. (C) Sacrificial template method [73] (with assistance of porous MXene spheres); reproduced with permission. Copyright 2017, Wiley and (D) ice template method with random [74]; reproduced with permission. Copyright 2019, Elsevier. (E) Unidirectional temperature gradient [13]; reproduced with permission. Copyright 2020, Elsevier. (F) Bidirectional temperature gradient [40]; reproduced with permission. Copyright 2019, Wiley.

freezing process. The growth speed of the ice crystal is affected by the surroundings of the solid/liquid interface, which is related to the properties of the solute and the whole solution condition, thereby determining the final structure of porous MXenes. In 2018, Liu's group [3] firstl fabricated MXene/rGO composite films via filtration and freeze-drying to maintain its porous structure. Later, Wang's group [9] formed 3D porous MXene aerogel through the freeze-drying method. Interestingly, it is confirmed that the pure MXene aerogel demonstrates small pores and tangles some networks [9, 74]. With the addition of rGO [7, 27], polyimide (PI) [82] and carbon nanotubes (CNTs) [25], the pore size of the hybrid aerogel increases and the structure gets ordered. Meanwhile, the crystal grows fast at extremely low temperatures, giving rise to porous MXenes with small pores. The pore size of the MXene aerogel frozen in a dry ice bath (−78 °C) [22] is larger than that in liquid nitrogen (−196 °C) [74].

Designing a unique temperature gradient is an efficient approach to control the structure of porous MXenes. A random cold environment facilitates the formation of uniform disordered porous structures due to the random growth of ice. In contrast, the networks become ordered under the condition that there is a specific temperature gradient. Generally, the unidirectional temperature gradient is favorable for the formation of structures with 1D columnar pores [13, 28, 34, 47, 49, 59, 85, 86], while the bidirectional temperature gradient tends to construct 2D layered porous structure [21, 23, 29, 40, 45]. Recently, many attempts have been made, and porous MXenes with various types of structure have been obtained. Zhang's group [13] created a unidirectional temperature gradient by attaching the molds filled with MXene/SA (sodium alginate) mixture to a copper cylinder, which was put into liquid nitrogen. Relevant fabrication processes are depicted in figure 2(E). In this process, considerable ice crystals

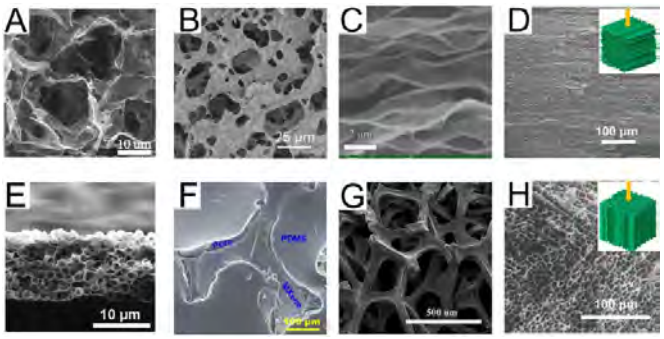

Figure 3. Various structures of 3D porous MXenes via different fabrication methods: (A) Cross-linking method [41]; reproduced with permission. Copyright 2019, American Chemical Society. (B) Cross-linking method [5]; Copyright 2019, Wiley. (C) Ice templating method [74]; reproduced with permission. Copyright 2019, Elsevier. (D), (H) Ice template method [13]; reproduced with permission. Copyright 2020, Elsevier. (E), (F) Sacrificial template method [73, 75]; reproduced with permission. Copyright 2019, Wiley. Copyright 2019, Elsevier. (G) Direct absorption method [67]; reproduced with permission. Copyright 2017, Elsevier.

are quickly formed at the bottom of the suspension and then grow along the direction of the temperature gradient. MXene sheets are repelled and aligned vertically, contributing to the fabrication of anisotropic micro-honeycomb porous MXenes (figures 3(D) and (H)). Additionally, porous MXenes with large directional channels were obtained similarly [86], whose pore size and number of 'bridges' can be changed by tuning the concentration of the solution: the higher the concentration is, the smaller the pores are. Although the ordered structure is realized by directional freezing, it is not sufficient to satisfy the requirements of practical applications. Porous MXenes with lamellar channels throughout the whole sample prepared by a dual-temperature gradient provide more possibilities. Bidirectional freezing is conducted in molds with a PDMS wedge at bottom (figure 2(F)) [21, 23, 40]. Similar to unidirectional freeing, the mixture solution is poured into a customized container and then placed on a cold plate (<0 °C). With the separation of the PDMS wedges, the temperature gradient of the system is inclined to the cold plate, which can be divided into vertical and horizontal directions, the so-called dual-temperature gradient. In this case, ice crystals appear only at the bottom of the wedge initially and then grow along the surface of the wedge in the vertical direction, confining the orientation of the vertical channels. After sublimation, porous MXenes with well-aligned a lamellar structure are fabricated successfully.

Apart from these aerogels, film-like MXene foams can also be fabricated by this method [3, 26, 31, 74, 78, 86–89]. Freeze-drying treatment after filtration retains the pores generated by the residual water in the hybrid film, resulting in film-like porous MXenes.

In general, compared with other methods, the ice template method shows better adaptability and simplification in the preparation process. The structure of MXenes can be easily tuned by adjusting the freezing conditions. In contrast, the direct absorption method is the simplest method, although the interface interaction between the MXenes and the templates still remains a problem. The emulsification method may be the most complex and demanding preparation process, but it is also the best way to improve the hydrophobicity of 3D porous MXenes. In addition, the cross-linking method shows more possibilities for regulation. Both the cross-linking initiators and the drying method can be further expanded and developed. Others such as the foaming method and the sacrificial template method are more limited and hard to be further explored.

3. Properties of porous MXenes

The physical chemical properties determine the final performance of the porous MXenes in practical applications. Density, porosity, conductivity, specific surface area (SSA) and some other properties are of particular concern as they collectively affect the performance of MXenes. Here, the underlying relationship between the properties and structures/materials is explored through the integration of these data as shown in figure 4.

3.1. Porosity, density, and SSA

Flexible and wearable electronic devices are widely used in daily life, and low-density porous MXenes can be a promising choice for the construction of wearable devices. As the pores of porous MXenes are filled with air, the porosity is inversely proportional to the density. It is obvious that the porosity merely depends on the porous structure of the MXenes, while their density is determined largely by the structures, rather than the materials. Commonly, the porosity of MXenes is larger than 99% for most fabrication methods. By comparing different structures of porous MXenes fabricated with the same material systems [6, 17, 22, 40, 72, 73], the density of film-like porous MXenes with ultra-small pores is hundreds of mg cm^{-3}, and those porous MXenes with large pores are below 100 mg cm^{-3} as shown in figure 4(A). As mentioned earlier, the concentration of the solution and types of additives cooperatively influence the pore size, and determine the density of porous MXenes [15, 16, 25, 79, 86].

Apart from the porosity and density, an ideal absorber or SC should hold high porosity and large SSA to offer numerous active sites. It is reported that porous MXenes with few-layer MXenes possess high SSA of about six folds of multi-layer MXenes. This phenomenon can be ascribed to the abundant exposed surface of few-layer MXenes [66]. Apart from the layers of MXenes, introducing other materials with high SSA can also improve the SSA of porous MXenes. For instance, the SSA of MXene/rGO hybrid foam is increased to 59.81 $m^2\ g^{-1}$ from 25.5 $m^2\ g^{-1}$ for MXene foam, while the SSA of rGO foam is 160.73 $m^2\ g^{-1}$, which is related to different expansion degrees of the foams [3]. In contrast to the SSA and pore sizes of different 3D porous MXenes, we find that their SSA decreases with the enlargement of their pore size, especially for aerogels fabricated by cross-linking method as shown in figure 4(B). This trend can be attributed to the fact that aerogels with relatively small pore size would expose more surfaces in the same volume, thus leading to higher SSA.

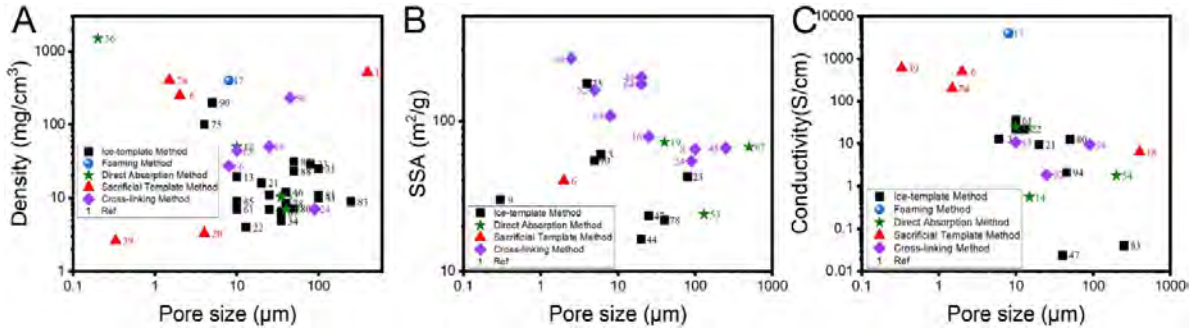

Figure 4. Relationship between the properties and the structures (pore size) of the porous MXenes.

3.2. Conductivity

Excellent conductivity renders MXene attractive in applications such as SCs, EMI shielding, and sensors. However, the formation of porous network structures introduces a tremendous gap, impeding the charge transport. In general, MXene films with larger pore size exhibit lower conductivity, as seen in figure 4(C). The conductivity of a typical MXene film is about 10^6 S m^{-1} and it decreases to 10^4 S m^{-1} when formed into a porous structure and further decreases with the increase in the pore sizes [17]. MXene aerogels fabricated by the ice template method show a conductivity as low as 376 S m^{-1} [72]. Besides, compounding some other materials imposes an adverse impact on the conductivity of porous MXenes, although they can improve their mechanical properties. For example, the addition of rGO into MXene foams decreases the conductivity from 2863 S cm^{-1} to 12.9 S cm^{-1} as a result of the larger expansion of rGO than MXene foams [3]. In addition, polymers such as PI [82], PVA [80], and PDMS [13] are frequently utilized to enhance the mechanical strength of porous MXenes; however, it interrupts the conductive networks and decreases their conductivity. It is worth noting that annealing treatment after the formation of the porous skeleton can improve the conductivity to some extent [3]. On the one hand, thermal treatment can reduce the GO or carbonize the carbon-based materials (such as cellulose, foams and so on), improving the intrinsic conductivity of the materials. On the other hand, annealing tightens the connection of the conductive network, further enhancing the electrical properties.

3.3. Mechanical properties

Mechanical properties should not be neglected as they determine the sensing range and life span of porous MXenes in practical applications. Porous MXenes with high Young's modulus, and strength, large compressibility and elasticity are desired in many applications. Generally, porous MXenes can withstand thousands of times their own weight [72] and show Young's modulus [90] of 0.01–15 GPa. Nevertheless, pure MXene aerogels tend to collapse under cyclic compressing and releasing process due to weak interaction between MXene lamellar structures [40]. To address this problem, considerable attempts have been made and many effective methods have been developed. Firstl, ordered porous structures can enhance the mechanical properties in certain directions. For instance, Sun's group [91] fabricated lamellar MXene/bacterial cellulose aerogels via uni-directional freeze-drying method and annealing treatment, improving their compressibility and elasticity in the direction perpendicular to the lamella direction. Compared with disordered MXene aerogel, the lamellar structure allowed the MXene/bacterial cellulose aerogel to retain its initial height and keep 94.5% of its original stress after 500 cycles at 50% strain. However, the Young's modulus of porous MXenes in the vertical direction and fatigue resistance in the parallel direction went through a significant decrease. In addition, graphene, cellulose, and polymers are effective additives to support the MXene sheets and provide elastic porous structure, which favors the improvement of Young's modulus and fatigue resistance. For example, the additive of graphene can not only endow MXene/GO/EDA aerogels with an high Young's modulus of 15 GPa and hardness of 0.7 GPa, but also improves their elasticity due to the outstanding mechanical properties of graphene. Cellulose also helps to build super compressive and elastic porous MXenes. In particular, bacterial cellulose shows the best optimization effect as reported by Sun's group [91]. It is worth noting that the addition of these low/non-conductive materials will bring about the loss of the conductivity of porous MXenes, limiting their application. Therefore, the types and proportions of additives should be carefully selected according to application requirements to balance the mechanical properties and conductivity. Meanwhile, elastic foams (NFs, PUFs, and so on) are superior substrates, which can serve as skeletons and provide wonderful compressibility and elasticity. Furthermore, PDMS can be injected into the pores of the porous MXenes to maintain their structures. After the infiltration, the strength and elasticity of porous MXenes are improved at the expense of density [13, 75].

3.4. Hydrophilicity

The hydrophilicity of MXenes limits their stability and reliability when used in environments with high humidity. In addition, hydrophobicity is beneficial for the improvement of their oil-absorption ability. Generally, the contact angle of MXene films is between 35° and 64°, making them easy to

absorb water and oxidize. In different fabrication processes, the contact angle of porous MXenes can be tuned between 82.3° and 135° [5, 11, 17, 72, 73]. For example, the hydrophilic groups on the surface of MXenes can be removed or occupied during annealing or grafting treatment, thus increasing their contact angle [17]. Russell's group also fabricated porous MXene aerogels via the emulsification method, which exhibit a large contact angle of 123° and improved oil-absorption performance. Such good hydrophobicity is due to the existence of hydrophobic POSS-NH_2 (polyhedral oligomeric silsesquioxane).

All in all the properties of 3D porous MXenes are dependent on their structures. Small pore size will result in large SSA, high conductivity, excellent Young's modulus and fatigue resistance, making 3D porous MXenes show excellent performance in various applications. However, low density and high porosity require large pore size. Hence, the pore size should be adjusted appropriately according to application requirements. In addition, ordered/gradient structure and suitable additives can be utilized for specific performance improvements.

4. Applications of porous MXenes

Porous MXenes combine the advantages of unique porous structures and excellent intrinsic properties of MXenes, making them promising in various applications. The main application fields of porous MXenes include EMI shielding, microwave absorption, energy conversion and storage, sensors, and so on.

4.1. EMI shielding or microwave absorption

With the rapid development of the electronic industry, electromagnetic waves of different wavelength permeate our daily life and can affect scientific experiments. Lightweight, wearable electronics with good EMI shielding and microwave absorption performance are highly desirable. It is reported that the conductivity (σ) and thickness (t) have a vital influence on the EMI SE as shown in formalism (1):

$$\mathrm{SE} = 50 + 10\log(\sigma/f) + 1.7t(\sigma)^{1/2}. \tag{1}$$

Here, σ (S cm^{-1}) is the conductivity, f (MHz) is the frequency of the electromagnetic wave, and t (cm) is the thickness. Therefore, high conductivity is beneficial to the electromagnetic reflection, while the porous structure provides multiple reflections to absorb the electromagnetic waves. Hence, the combination of porous structure and high electrical conductivity of MXenes makes porous MXenes promising for EMI shielding.

As reported by Gogotsi *et al*, a 45 μm MXene film shows an excellent EMI-SE of >92 dB due to its high conductivity and abundant surface groups. Later, Zhang's group confirmed that its SE would be reduced with a decrease in thickness, and the formation of a porous network contributes to the improvement of EMI-SE from 53 dB for the MXene film to 70 dB for its foamed counterpart as shown in figures 5(G) and (H) [17].

In other words, porous MXenes exhibit better SE than MXene films with the same number of MXene sheets, proving that the construction of porous structures can maximize the utilization of the MXenes. These examples indicate that the structure of porous MXenes plays a significant role in the EMI shielding process. A general relationship between the structure and EMI-SE is concluded: the SE of porous MXenes with a lamellar porous network is highest, a columnar porous structure comes second, and lowest is a disordered skeleton. In addition, introducing conductive materials (such as CNT, metal nanowires and so on) into porous MXenes could improve their SE. However, good mechanical properties are also required in practical applications. As mentioned earlier, many additives (graphene, cellulose, and so on) would decrease the conductivity of porous MXenes and increase the elasticity. To circumvent this dilemma, thermal treatment is applied to carbonize or reduce these additives, and succeeds in promoting the conductivity and maintaining the fatigue resistance. For instance, an ultra-high EMI SE reaches up to 103.9 dB after the CNTs-enabled formation of bridged lamellar structures (figure 5(I)) [21].

Compared with EMI-shielding, the requirements for microwave absorption are more stringent. To evaluate the absorption performance of these materials, the microwave reflection loss (RL) performance can be calculated using the following formulas:

$$Z_{\mathrm{in}} = \sqrt{\frac{\mu_{\mathrm{r}}}{\varepsilon_{\mathrm{r}}}}\tanh\left(j\frac{2\pi fd}{c}\sqrt{\mu_{\mathrm{r}}\varepsilon_r}\right) \tag{2}$$

$$\mathrm{RL} = 20\log 10\left|\frac{Z_{\mathrm{in}}-1}{Z_{\mathrm{in}}+1}\right|. \tag{3}$$

Here, Z_{in} is the normalized input impedance of absorbing materials, d is their thickness, ε and μ are their complex permittivity and permeability, respectively, f is the frequency of the electromagnetic wave, and c is the speed of light in vacuum. In detail, RL below −10 dB denotes that more than 90% electromagnetic energy is absorbed, while −20 dB denotes that more than 99% is absorbed. In addition, the bandwidth with reflection less than −10 dB is termed as the effective absorption bandwidth, which represents the absorption ability of the materials.

According to the formulas, moderate conductivity, suitable impedance and optimized structure allow good microwave absorbtion performance with broadband absorption and excellent absorbtionefficiency as shown in figures 5(D) and (F). In principle, a relatively low conductivity is beneficial to the entry of the microwave, while porous structures allow their multi-reflection. Hence, the negative effect of the additives (cellulose, rGO, etc) on the conductivity of porous MXenes is turned into an advantage. The combination of their porous structure and adjustability of their conductivity by modifying MXenes or compounding other materials endows most of the porous MXenes with an excellent microwave RL performance within a wide absorption range from 8.2 to 12.4 Hz [16, 20, 23, 25, 41, 64, 80, 82]. For instance, Yin's group constructed rGO/MXene-based hollow core–shell architectures

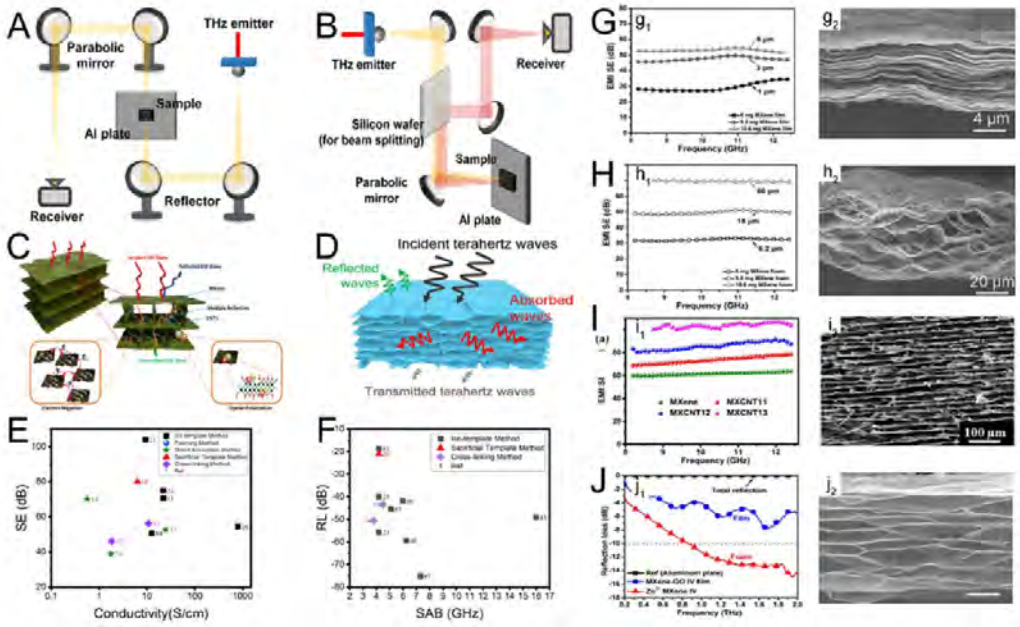

Figure 5. (A), (B) The schematic of the measuring instrument of EMI/MA performance [16]. (C), (D) Schematic illustration of the EMI shielding and MA mechanism of the porous MXenes [16, 21]; reproduced with permission. Copyright 2019, American Chemical Society. (E) Relationship between EMI SE and conductivity of the porous MXenes. (F) Comparison of the microwave reflection loss (RL) performance and effective absorption bandwidth (SAB) of the porous MXenes [16]. (G), (H) EMI shielding performance of the porous MXenes and their corresponding structures [17, 21]: hydrophobic MXene films (G)/foams (H); MXene/CNT hybrid aerogels (I); reproduced with permission. Copyright 2017, Wiley. (J) MA performance of the MXene aerogels fabricated by cross-linking method with assistant of metal foils [16] and their structures; (A), (B), (F), (J) reproduced with permission. Copyright 2020, American Chemical Society.

with sphere-like porous structure and suitable permittivity, achieving an excellent absorption performance (<−20 dB). Later, they found that decreasing the dosage of the conductive MXene could increase their RL from −6.7 to −18.7 dB. Meanwhile, it was confirmed that the introduction of porous structures would decrease their conductivity, thereby increasing the absorption performance and decreasing the EMI ability.[79] With the same content, the MXene/PVA composite foams show lower SE_R (2 dB) than the films (14 dB, which was obtained by compressing the foams twice). Surprisingly, a super-wide absorption range (0.2–2.0 THz) is realized by the formation of a MXene/GO hybrid aerogel with a porous structure and its RL reaches −37 dB (figure 5(J)) [41]. In addition, it is also a viable method to composite 3D porous MXenes with magnetic materials or design a structure/composition gradient. The former could improve the magnetic relaxation loss, while the latter would allow more electromagnetic waves to enter and dissipate them internally.

4.2. Energy conversion and storage

In recent years, energy deficiency has become one of the major problems that plagues human development in the world. Meanwhile, the arrival of the age of intelligence promotes the development of electronics toward the direction of miniaturization, light weight and wearability. Therefore, the development of flexible energy storage devices is stimulated vigorously. Excellent electro-chemical properties and high SSA make porous MXenes promising to serve as flexible electrodes in energy storage systems, such as SCs (figures 6(A)–(F)) and various rechargeable ion batteries (figures 6(G)–(J)).

As a crucial type of energy storage device, SCs attract tremendous attention because of their high energy density, long lifetime and excellent cycling capability. Generally, the specific capacity of SCs is related to their SSA, which is associated with the structure of porous MXenes and natural properties of raw materials. The porous structure facilitates full contact between the electrode material and the electrolyte, which can accelerate the diffusion of ions.In addition, large SSA can provide more electrochemically active sites, thereby achieving higher specific energy/specific power. In the meantime, high conductivity enables fast electron transfer. By employing a 3D porous architecture, Liu's group [4] prepared a Co_3O_4-MXene/rGO hybrid aerogel-based SC with high specific capacitance (345 F g^{-1}) as shown in figures 6(A)–(C). In addition, Zhang's group [65] fabricated MXene aerogels with a high special capacitance of 438 F g^{-1} and a high capacitance retention of 90% after 20 000 charging–discharging cycles. The high specific capacitance and high cycling performance can be put down to the unique 3D porous structure, which inhibits the re-stacking of MXene sheets and enhances the surface area. With the support of Ni foam, the capacitance performance of porous MXenes is greatly improved. Zhao's group [27] prepared porous MXenes through the deposition of MXene onto NF and a high specific capacity of 654 F g^{-1} was obtained. Later, with *in*

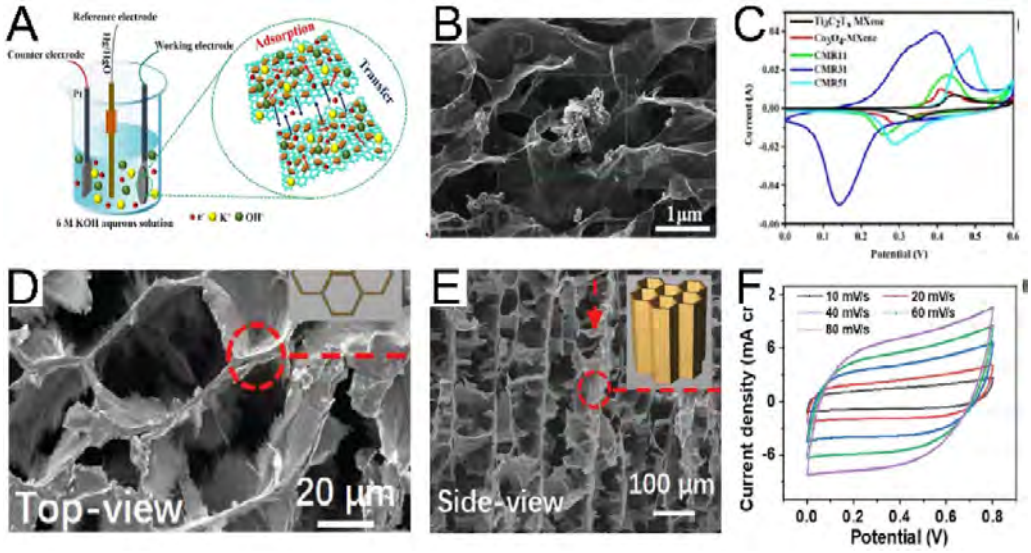

Figure 6. Energy conversion and storage applications of the porous MXenes. (A)–(C) Working mechanism, structure and capacity performance of the Co3O4-MXene/rGO hybrid aerogel based super capacitors [4]; reproduced with permission. Copyright 2019, Wiley. (D)–(F) Ordered structure and capacity performance of the MXene aerogel fabricated by 3D printing and freeze-drying [92]; reproduced with permission. Copyright 2020, Wiley.

situ formation of Ni_3S_2 on the MXene/NF composite, they improve the performance of the porous MXenes to 2204 F g^{-1} with synergistic effect of Ni_3S_2 and MXene [2]. The composite takes the advantages of the high energy density of Ni_3S_2 and high conductivity of MXene. Unfortunately, the cycling stability of SCs are reduced with the existence of NF. The retention of MXene/NF and Ni_3S_2/MXene/NF are 80.6% and 76.3% after 5000 cycles, respectively. Moreover, Liang's group formed a 3D porous MXene scaffold by 3D printing and freeze-drying recently. They exhibit excellent areal capacitance (216.2 mF cm^{-2}) and good stability (almost no decay after 1000 stretch/release cycles) as shown in figures 6(D)–(F).

Considerable research work has been done on batteries, such as Li–S batteries (LSBs) and Li-ion batteries (LIBs) in recent years, and porous MXenes are attractive candidates as electrodes. Like SCs, the performance of batteries can be enhanced by high electrode conductivity and large surface area. However, there are still many challenges to improve the performance of LSBs: shuttle of lithium polysulfides (LiPSs), volume expansion and natural insulating properties of elemental sulfur, and so on. Wang's group reported a MXene/rGO aerogel with high capacity of 1270 mA × h g^{-1} and outstanding stability (only 0.07% capacity decay after 500 cycles). In addition, a 3D MnO_2 nanosheet/MXene aerogel is fabricated to serve as a sulfur host for LSB cathodes [10]. The synergistic effect of the two components renders the accommodation of the elemental sulfur and confines the dissolution of LiPSs, thus endowing LSBs with a high initial specific discharge capacity of 1140 mA × h g^{-1} and 91% capacity retention after 500 cycles. Abundant ion transfer and plenty of available intercalating sites are required for an ideal LIB. Zhou's group [8] dispersed MXene sheets onto rGO sheets and formed a 3D porous structure by cross-linking method. The MXene/rGO hybrid aerogel exhibits a capacity of 357 mA × h g^{-1} as an anode of LIBs.

4.3. Sensors

At present, flexible and compressible bionic sensing electronic devices have attracted wide attention in the fields of human–computer interaction interface, electronic skin and human health monitoring. The 3D porous architecture and excellent conductivity make porous MXenes competitive in the application of flexible sensors. Here, we arrange the relevant information of porous MXenes based sensors with different frameworks and materials as listed in Table 1. As shown in figure 7(A), they can efficiently capture subtle deformation signals and convert them into electrical signals, realizing the sensing of the external environment. Sensitivity (S) can be calculated by formula (4):

$$S = \frac{\delta(\Delta I/I_0)}{\delta P}. \tag{4}$$

Here, ΔI is the relative variety of the current under compression, I_0 is the initial current without pressure, and P is the applied pressure. Nevertheless, it is hard to achieve high sensitivity (S) and broad sensing range simultaneously. Generally, high sensitivity requires resistance of porous MXenes and changes a lot under small pressure, while a broad sensing range requires continuous changes in a wide range, which are mutually restrictive. Therefore, porous MXenes with high sensitivity (>100 kPa^{-1}) always show a limited sensing range (<10 kPa), and vice versa. In addition, stability is another important evaluation indicator for sensor performance, which is closely related to mechanical properties. Generally, porous MXene-based sensors can maintain their current response

Table 1. Performance of PMs in sensors.

Materials	Structure	Sensitivity (kPa^{-1})	Cycle	Limit	Range	References
$Ti_3C_2T_x$/rGO	Lamellar	22.56	10 000	10 Pa	—	[27]
$Ti_3C_2T_x$/CS/PU	Template-like	0.001–0.015	5000	9 Pa	245.7 kPa	[69]
$Ti_3C_2T_x$/PDMS	Ordered	Weight	1000	10 mg	10–600 mg	[75]
$Ti_3C_2T_x$/rGO	Directional	0.28	—	60	66.98	[59]
$Ti_3C_2T_x$/ANF	Lamellar	128	—	100	623	[31]
$Ti_3C_2T_x$/Fe_3O_4/GPN/Ecoflex	Template-like	4.71	—	—	0–62.5	[30]
$Ti_3C_2T_x$ Sphere/rGO	Disordered	609	6000	6	0–10	[32]
PINF/$Ti_3C_2T_x$	Lamellar	0.14	1000	10	85.21	[33]
$Ti_3C_2T_x$/rGO/Fe_3O_4/Ni/PDMS	Template-like	0.12	—	—	—	[18]
$Ti_3C_2T_x$/AgNWs	Lamellar	645.6	1000	1.25	0–9	[29]
$Ti_3C_2T_x$/CNC	Lamellar	114.6	10 000	1	0–10	[28]
$Ti_3C_2T_x$/CNF/PVP	Directional	65	5000	5	0%–95%	[34]

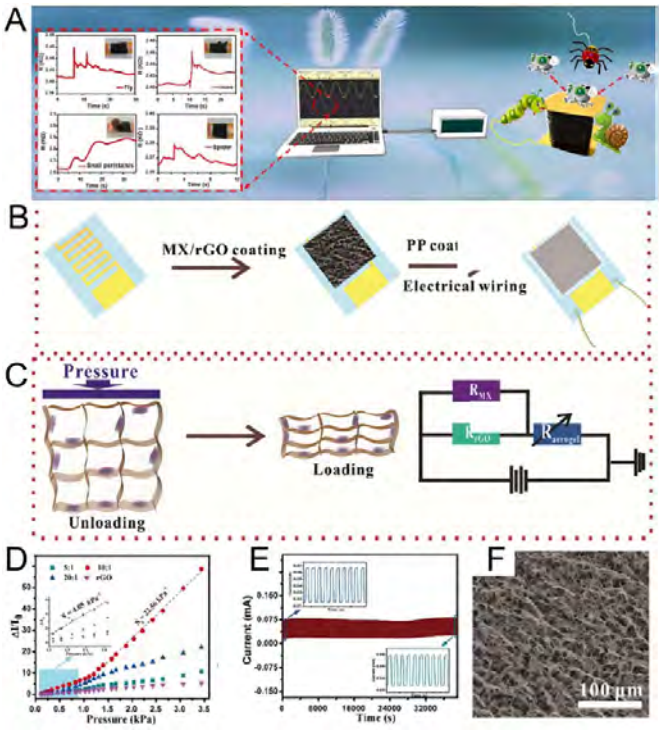

Figure 7. Operating process (A) [69]; reproduced with permission. Copyright 2019, Elsevier. Fabrication process (B) and sensing mechanism (C) [27] of the porous MXenes based pressure sensor; sensing performance and structures of different porous MXenes: 3D MXene/rGO aerogels (D)–(F) [27]; reproduced with permission. Copyright 2018, American Chemical Society.

after 1000–10 000 cycles of compression under a relatively low pressure.

Ordered porous structures and suitable materials (graphene, CNT, cellulose, etc) can improve their electronic conductivity and mechanical properties, thereby improving their performance as pressure sensors. As reported by Gao's group, MXene/rGO aerogels fabricated by the ice template method display a high sensitivity of 22.56 kPa^{-1}, an ultra-low detection limit of 10 Pa, and excellent durability of 10 000 cycles at 510 Pa (figures 7(D)–(F)) [93].

During compression, deformation of the network of the MXene/rGO aerogel contributes to an increased number of conductive paths and thus improves the conductivity of the 3D monoliths, which is the main operating mechanism of piezoresistive sensors. However, their working range is limited below 3.5 kPa, which is not enough in many practical applications. To broaden the sensing range of porous MXenes, a PU foam is employed to support the conductive MXene nanosheets, achieving a super wide working range (0–245.7 kPa) at the cost of sensitivity (0.001–0.015 kPa^{-1}). Additionally, it is reported that the durability of porous MXene-based sensors can be optimized through composition with cellulose, and bacterial cellulose offers the best efficacy [91].

These excellent properties result in a high sensitivity of 12.5 kPa^{-1} and a long operating life of 1000 cycles at 50% strain. It is worth noting that all porous MXene-based sensors show ultra-low sensing limits (the lowest pressure the sensor can detect) (1–10 Pa), making them promising for physiological signal monitoring applications.

4.4. Other applications

The porous structure also makes porous MXenes a promising candidate for thermal insulation and solar steam generation. Several related applications have been shown in figure 8. Barg's group [94] found that MXene/epoxy aerogel composites show excellent electro-thermal properties. They can achieve a high power output (6.1 W cm^{-2}) at a 2 V voltage, which corresponds to 123 °C Joule heating performance. In addition, Yu's group [82] fabricated a porous MXene/PI aerogel by the freeze-drying method, showing unique thermal resistance with positive inflmuence of PI and flame retardation of the hybrid aerogel as shown in figures 8(A)–(C). Chen's group [54] prepared porous MXene aerogels with pomelo peels as a template. After mixed with PEG and thermal treatment, the composites show excellent light-thermal conversion and storage performance. Their surface temperature would increase to 84.3 °C from room temperature under irradiation of the light (figures 8(D)–(F)). In addition, Yang's group [71] fabricated a 3D MXene/PVA/MF architecture with a water evaporation rate of 7.49 kg m^{-2} × h and an ultra-high solar steam efficiency of 94.2% under solar illumination of 5 suns. The excellent solar steam generation performance

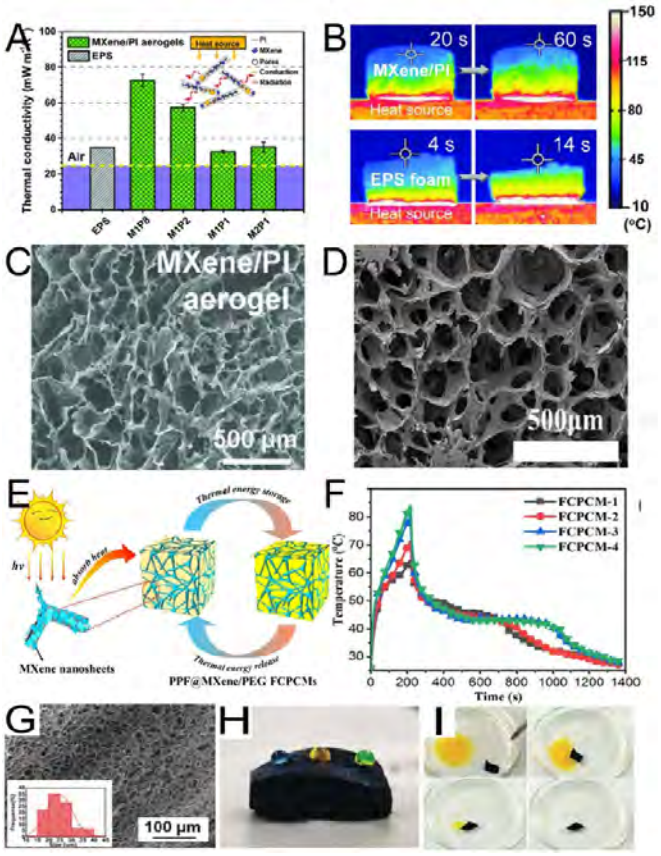

Figure 8. Other applications of the porous MXenes. (A)–(C) Thermal insulation performance and their structure of the MXene/PI composites [82]; reproduced with permission. Copyright 2018, Wiley. (D)–(F) Schematic illustration of thermal energy conversion and storage performance of the PPF@MXene/PEG composites and their structure [54]; reproduced with permission. Copyright 2020, Elsevier. (G)–(I) Structure and oil absorption performance of the MXene foams fabricated by emulsification method [72]; reproduced with permission. Copyright 2019, Wiley.

of the hybrid relies on the intrinsic hydrophilicity of MXenes and the macro-porous structure of the aerogel. Furthermore, the porous structure and suitable hydrophobic surface endow porous MXenes with excellent oil absorption performance (figures 8(G)–(I)) [72]. Efficient capacitive deionization and ultrahigh removal of mercuric ions can also be achieved respectively.

In general, large SSA endows 3D porous MXenes with excellent energy storage capability, while high conductivity, excellent fatigue resistance and porous structure are conducive to the improvement of their performance in EMI shielding and sensor applications. In addition, low density and high hydrophobicity can be achieved by adjusting the structure of 3D porous MXenes, making them more suitable for practical applications.

5. Conclusion and outlook

A considerable number of studies have focussed on porous MXenes since their first synthesis in 2011. Porous MXenes with various structures have been fabricated by the foaming method, cross-linking method, and template method. They also exhibit high electrical conductivity, good mechanical properties, and hydrophobicity. It is worth noting that ordered pores with suitable size lead to high conductivity, large SSA and excellent fatigue resistance. The combination of these merits makes porous MXenes exceptionally promising in a broad range of application fields. In terms of electromagnetic shielding, high conductivity and multiple reflection caused by porous structures endow porous MXenes with excellent SE as high as 103.9 dB. As for microwave absorption, tuneable conductivity and suitable permittivity are conducive to the absorption of electromagnetic waves instead of reflection, thereby achieving excellent RL (−75.2 dB) or broad absorbing range (0.2–2 THz). Besides, large SSA is beneficial to the improvement of energy conversion and storage performance. A 2204 F g^{-1} specific capacity was obtained with lamellar structure. With regard to sensors, porous structure provides fewer conductive paths initially and broadened compressible range, thus improving their sensitivity as high as 645.6 $kPa^{-1}$and sensing range as broad as 245.7 kPa. Nevertheless, the development of porous MXenes still face several challenges.

First, it is still a formidable challenge to achieve precise control of the micro- and macrostructure of porous MXenes. Although various fabrication methods have been reported previously as introduced above, the structure of porous MXenes cannot be tuned accurately for details such as pore size and interlayer spacing. At the same time, a unique hierarchical structure cannot be constructed which may be beneficial to the performance of porous MXene-based sensors or EMI-shielding. In-depth studies on the influence of precursor solution conditions and external environment on structures may provide a solution to this challenge.

Secondl, the relationship between structure and property has been roughly concluded previously. However, it is not clear enough to guide the structure design in target applications due to the difference in raw materials and test conditions in the literature. Therefore, relevant research with a single variable is needed to direct the fabrication of porous MXenes with the desired properties. In addition, simulation and modeling analysis may be helpful.

Furthermore, the porous structure separates the conductive paths and exposes more surface area, making it difficult for porous MXenes to improve conductivity and enlarge the SSA synergistically. Meanwhile, satisfactory mechanical properties such as superb elasticity and fatigue resistance are still out of reach due to the weak interaction between the MXene sheets and additives. All these properties have a crucial influence on the performance of porous MXenes in practical use. Hence, more efforts are required to balance these properties to fabricate a porous MXene with desired performance.

More importantly, the excellent SSA and mechanical properties make 3D porous MXenes promising to be used in catalysis, adsorption, medical and other applications, which has been proven to be feasible with graphene-based aerogels [95]. However, related research in 3D porous MXenes is still lacking. More application scenarios are still to be explored.

Finally, there also remains a challenge in transitioning from laboratory to practical applications. For instance, the temperature, humidity, and pressure may influence the performance and lifespan of the devices in daily use. Extensive efforts are needed to make the porous MXene-based devices mature.

Data availability statement

No new data were created or analysed in this study.

Acknowledgments

This work was supported by the Youth Innovation Promotion Association CAS (Y201841); National Natural Science Foundation of China (61871368); Austrian-Chinese Cooperative R&D projects (GJHZ2046); Instrument and equipment development program sponsored by CAS (YJKYYQ20180065).

ORCID iDs

Ranran Wang https://orcid.org/0000-0001-5097-2834
Jing Sun https://orcid.org/0000-0002-9810-9551

References

[1] Naguib M, Kurtoglu M, Presser V, Lu J, Niu J, Heon M, Hultman L, Gogotsi Y and Barsoum M W 2011 Two-dimensional nanocrystals produced by exfoliation of Ti_3AlC_2 *Adv. Mater.* **23** 4248–53
[2] Zhao Y, Guo J, Liu A and Ma T 2020 2D heterostructure comprised of Ni_3S_2/d-Ti_3C_2 supported on Ni foam as binder-free electrode for hybrid supercapacitor *J. Alloys Compd.* **814** 152271
[3] Ma Z, Zhou X, Deng W, Lei D and Liu Z 2018 3D porous MXene (Ti_3C_2)/reduced graphene oxide hybrid films for advanced lithium storage *ACS Appl. Mater. Interfaces* **10** 3634–43
[4] Liu R, Zhang A, Tang J, Tian J, Huang W, Cai J, Barrow C, Yang W and Liu J 2019 Fabrication of cobaltosic oxide nanoparticle-doped 3D MXene/graphene hybrid porous aerogels for all-solid-state supercapacitors *Chemistry* **25** 5547–54
[5] Deng Y *et al* 2019 Fast gelation of $Ti_3C_2T_x$ MXene initiated by metal ions *Adv. Mater.* **31** e1902432
[6] Zhao Q, Zhu Q, Miao J, Zhang P, Wan P, He L and Xu B 2019 Flexible 3D porous MXene foam for high-performance lithium-ion batteries *Small* **15** e1904293
[7] Yue Y *et al* 2018 Highly self-healable 3D microsupercapacitor with MXene-graphene composite aerogel *ACS Nano* **12** 4224–32
[8] Butt R, Siddique A H, Bokhari S W, Jiang S, Lei D, Zhou X and Liu Z 2019 Niobium carbide/reduced graphene oxide hybrid porous aerogel as high capacity and long-life anode material for Li-ion batteries *Int. J. Energy Res.* **43** 4995–5003
[9] Bao W, Tang X, Guo X, Choi S, Wang C, Gogotsi Y and Wang G 2018 Porous cryo-dried MXene for efficient capacitive deionization *Joule* **2** 778–87
[10] Zhang H, Qi Q, Zhang P, Zheng W, Chen J, Zhou A, Tian W, Zhang W and Sun Z 2018 Self-assembled 3D MnO_2 nanosheets@delaminated-Ti_3C_2 aerogel as sulfur host for lithium–sulfur battery cathodes *ACS Appl. Energy Mater.* **2** 705–14
[11] Shi L, Lin S, Li L, Wu W, Wu L, Gao H and Zhang X 2018 $Ti_3C_2T_x$-foam as free-standing electrode for supercapacitor with improved electrochemical performance *Ceramics Int.* **44** 13901–7
[12] Weng C, Wang G, Dai Z, Pei Y, Liu L and Zhang Z 2019 Buckled AgNW/MXene hybrid hierarchical sponges for high-performance electromagnetic interference shielding *Nanoscale* **11** 22804–12
[13] Wu X, Han B, Zhang H-B, Xie X, Tu T, Zhang Y, Dai Y, Yang R and Yu Z-Z 2020 Compressible, durable and conductive polydimethylsiloxane-coated MXene foams for high-performance electromagnetic interference shielding *Chem. Eng. J.* **381** 122622
[14] Li S, Wang J, Zhu Z, Liu D, Li W, Sui G and Park C B 2021 CVD carbon-coated carbonized loofah sponge loaded with a directionally arrayed MXene aerogel for electromagnetic interference shielding *J. Mater. Chem.* A **9** 358–70
[15] Zhao S, Zhang H-B, Luo J-Q, Wang Q-W, Xu B, Hong S and Yu Z-Z 2018 Highly electrically conductive three-dimensional $Ti_3C_2T_x$ MXene/reduced graphene oxide hybrid aerogels with excellent electromagnetic interference shielding performances *ACS Nano* **12** 11193–202
[16] Lin Z, Liu J, Peng W, Zhu Y, Zhao Y, Jiang K, Peng M and Tan Y 2020 Highly stable 3D $Ti_3C_2T_x$ MXene-based foam architectures toward high-performance terahertz radiation shielding *ACS Nano* **14** 2109–17
[17] Liu J, Zhang H-B, Sun R, Liu Y, Liu Z, Zhou A and Yu Z-Z 2017 Hydrophobic, flexible, and lightweight MXene foams for high-performance electromagnetic-interference shielding *Adv. Mater.* **29** 1702367
[18] Nguyen V-T, Min B K, Yi Y, Kim S J and Choi C-G 2020 MXene($Ti_3C_2T_X$)/graphene/PDMS composites for multifunctional broadband electromagnetic interference shielding skins *Chem. Eng. J.* **393** 124608
[19] Wang Y, Yang J, Chen Z and Hu Y 2019 A new flexible and ultralight carbon foam/$Ti_3C_2T_X$ MXene hybrid for high-performance electromagnetic wave absorption *RSC Adv.* **9** 41038–49
[20] Li X, Yin X, Song C, Han M, Xu H, Duan W, Cheng L and Zhang L 2018 Self-assembly core-shell graphene-bridged hollow MXenes spheres 3D foam with ultrahigh specific EM absorption performance *Adv. Funct. Mater.* **28** 1803938
[21] Sambyal P, Iqbal A, Hong J, Kim H, Kim M-K, Hong S M, Han M, Gogotsi Y and Koo C M 2019 Ultralight and mechanically robust $Ti_3C_2T_x$ hybrid aerogel reinforced by carbon nanotubes for electromagnetic interference shielding *ACS Appl. Mater. Interfaces* **11** 38046–54
[22] Bian R, He G, Zhi W, Xiang S, Wang T and Cai D 2019 Ultralight MXene-based aerogels with high electromagnetic interference shielding performance *J. Mater. Chem.* C **7** 474–8
[23] Li X, Yin X, Xu H, Han M, Li M, Liang S, Cheng L and Zhang L 2018 Ultralight MXene-coated, interconnected SiCnws three-dimensional lamellar foams for efficient microwave absorption in the X-band *ACS Appl. Mater. Interfaces* **10** 34524–33
[24] Hu K, Wang H, Zhang X, Huang H, Qiu T, Wang Y, Zhang C, Pan L and Yang J 2021 Ultralight $Ti_3C_2T_x$ MXene foam with superior microwave absorption performance *Chem. Eng. J.* **408** 127283
[25] Liu X, Chai N, Yu Z, Xu H, Li X, Liu J, Yin X and Riedel R 2019 Ultra-light, high flexible and efficient CNTs/Ti_3C_2-sodium alginate foam for electromagnetic absorption application *J. Mater. Sci. Technol.* **35** 2859–67
[26] Zhou Z, Liu J, Zhang X, Tian D, Zhan Z and Lu C 2019 Ultrathin MXene/calcium alginate aerogel film for

high-performance electromagnetic interference shielding *Adv. Mater. Interfaces* **6** 1802040
[27] Ma Y *et al* 2018 3D synergistical MXene/reduced graphene oxide aerogel for a piezoresistive sensor *ACS Nano* **12** 3209–16
[28] Zhuo H, Hu Y, Chen Z, Peng X, Liu L, Luo Q, Yi J, Liu C and Zhong L 2019 A carbon aerogel with super mechanical and sensing performances for wearable piezoresistive sensors *J. Mater. Chem.* A **7** 8092–100
[29] Bi L, Yang Z, Chen L, Wu Z and Ye C 2020 Compressible AgNWs/$Ti_3C_2T_x$ MXene aerogel-based highly sensitive piezoresistive pressure sensor as versatile electronic skins *J. Mater. Chem.* A **8** 20030–6
[30] Mondal S, Min B K, Yi Y, Nguyen V-T and Choi C-G 2021 Gamma-ray tolerant flexible pressure–temperature sensor for nuclear radiation environment *Adv. Mater. Technol.* **6** 2001039
[31] Wang L, Zhang M, Yang B, Tan J and Ding X 2020 Highly compressible, thermally stable, light-weight, and robust aramid nanofibers/Ti_3AlC_2 MXene composite aerogel for sensitive pressure sensor *ACS Nano* **14** 10633–47
[32] Zhu M *et al* 2019 Hollow MXene sphere/reduced graphene aerogel composites for piezoresistive sensor with ultra-high sensitivity *Adv. Electron. Mater.* **6** 1901064
[33] Liu H *et al* 2021 Lightweight, superelastic, and hydrophobic polyimide nanofiber/MXene composite aerogel for wearable piezoresistive sensor and oil/water separation applications *Adv. Funct. Mater.* **31** 2008006
[34] Qin L, Yang D, Zhang M, Zhao T, Luo Z and Yu Z-Z 2021 Superelastic and ultralight electrospun carbon nanofiber/MXene hybrid aerogels with anisotropic microchannels for pressure sensing and energy storage *J. Colloid Interface Sci.* **589** 264–74
[35] Yao M, Chen Y, Wang Z, Shao C, Dong J, Zhang Q, Zhang L and Zhao X 2020 Boosting gravimetric and volumetric energy density via engineering macroporous MXene films for supercapacitors *Chem. Eng. J.* **395** 124057
[36] Fang Y *et al* 2020 Porous and free-standing Ti_3C_2T-RGO film with ultrahigh gravimetric capacitance for supercapacitors *Chin. Chem. Lett.* **31** 1004–8
[37] Miao J, Zhu Q, Li K, Zhang P, Zhao Q and Xu B 2021 Self-propagating fabrication of 3D porous MXene-rGO film electrode for high-performance supercapacitors *J. Energy Chem.* **52** 243–50
[38] Li K, Wang X, Li S, Urbankowski P, Li J, Xu Y and Gogotsi Y 2020 An ultrafast conducting polymer@MXene positive electrode with high volumetric capacitance for advanced asymmetric supercapacitors *Small* **16** e1906851
[39] Yang M, Yuan Y, Li Y, Sun X, Wang S, Liang L, Ning Y, Li J, Yin W and Li Y 2020 Anisotropic electromagnetic absorption of aligned $Ti_3C_2T_x$ MXene/gelatin nanocomposite aerogels *ACS Appl. Mater. Interfaces* **12** 33128–38
[40] Han M *et al* 2019 Anisotropic MXene aerogels with a mechanically tunable ratio of electromagnetic wave reflection to absorption *Adv. Opt. Mater.* **7** 1900267
[41] Ma W, Chen H, Hou S, Huang Z, Huang Y, Xu S, Fan F and Chen Y 2019 Compressible highly stable 3D porous MXene/GO foam with a tunable high-performance stealth property in the terahertz band *ACS Appl. Mater. Interfaces* **11** 25369–77
[42] Li Y, Meng F, Mei Y, Wang H, Guo Y, Wang Y, Peng F, Huang F and Zhou Z 2020 Electrospun generation of $Ti_3C_2T_x$ MXene@graphene oxide hybrid aerogel microspheres for tunable high-performance microwave absorption *Chem. Eng. J.* **391** 123512
[43] Feng Y, Wang H, Xu J, Du X, Cheng X, Du Z and Wang H 2021 Fabrication of MXene/PEI functionalized sodium alginate aerogel and its excellent adsorption behavior for Cr(VI) and Congo Red from aqueous solution *J. Hazard. Mater.* **416** 125777
[44] Maleki H, Fischer T, Bohr C, Auer J, Mathur S and Milow B 2021 Hierarchically organized biomimetic architectured silk fibroin-ceramic-based anisotropic hybrid aerogels for thermal energy management *Biomacromolecules* **22** 1739–51
[45] Dai Y, Wu X, Liu Z, Zhang H-B and Yu Z-Z 2020 Highly sensitive, robust and anisotropic MXene aerogels for efficient broadband microwave absorption *Composites* B **200** 108263
[46] Zhang P *et al* 2020 *In situ* ice template approach to fabricate 3D flexible MXene film-based electrode for high performance supercapacitors *Adv. Funct. Mater.* **30** 2000922
[47] Zhang Q, Yi G, Fu Z, Yu H, Chen S and Quan X 2019 Vertically aligned janus MXene-based aerogels for solar desalination with high efficiency and salt resistance *ACS Nano* **13** 13196–207
[48] Shang T, Lin Z, Qi C, Liu X, Li P, Tao Y, Wu Z, Li D, Simon P and Yang Q-H 2019 3D macroscopic architectures from self-assembled MXene hydrogels *Adv. Funct. Mater.* **29** 1903960
[49] Yu Z and Wu P 2020 Biomimetic MXene-polyvinyl alcohol composite hydrogel with vertically aligned channels for highly efficient solar steam generation *Adv. Mater. Technol.* **5** 2000065
[50] Xie X, Wu Z and Zhang N 2020 Robust and easily retrievable Pd/$Ti_3C_2T_x$⊂graphene hydrogels for efficient catalytic hydrogenation of nitroaromatic compounds *Chin. Chem. Lett.* **31** 1014–7
[51] Zhang L and Or S W 2020 Self-assembled three-dimensional macroscopic graphene/MXene-based hydrogel as electrode for supercapacitor *APL Mater.* **8** 091101
[52] Shi H *et al* 2020 3D flexible, conductive, and recyclable $Ti_3C_2T_x$ MXene-melamine foam for high-areal-capacity and long-lifetime alkali-metal anode *ACS Nano* **14** 8678–88
[53] Sang M, Wu Y, Liu S, Bai L, Wang S, Jiang W, Gong X and Xuan S 2021 Flexible and lightweight melamine sponge/MXene/polyborosiloxane (MSMP) hybrid structure for high-performance electromagnetic interference shielding and anti-impact safe-guarding *Composites* B **211** 108669
[54] Sheng X, Dong D, Lu X, Zhang L and Chen Y 2020 MXene-wrapped bio-based pomelo peel foam/polyethylene glycol composite phase change material with enhanced light-to-thermal conversion efficiency, thermal energy storage capability and thermal conductivity *Composites* A **138** 106067
[55] Wu Z, Shang T, Deng Y, Tao Y and Yang Q-H 2020 The assembly of MXenes from 2D to 3D *Adv. Sci.* **7** 1903077
[56] Bu F, Zagho M M, Ibrahim Y, Ma B, Elzatahry A and Zhao D 2020 Porous MXenes: synthesis, structures, and applications *Nano Today* **30** 100803
[57] Zhang X, Lv R, Wang A, Guo W, Liu X and Luo J 2018 MXene aerogel scaffolds for high-rate lithium metal anodes *Angew. Chem., Int. Ed. Engl.* **57** 15028–33
[58] Song J, Guo X, Zhang J, Chen Y, Zhang C, Luo L, Wang F and Wang G 2019 Rational design of free-standing 3D porous MXene/rGO hybrid aerogels as polysulfide reservoirs for high-energy lithium–sulfur batteries *J. Mater. Chem.* A **7** 6507–13
[59] Jiang D, Zhang J, Qin S, Wang Z, Usman K A S, Hegh D, Liu J, Lei W and Razal J M 2021 Superelastic $Ti_3C_2T_x$ MXene-based hybrid aerogels for compression-resilient devices *ACS Nano* **15** 5000–10
[60] N R, A. K, H.m. M, M.r. N, Mondal D, Nataraj S K and Ghosh D 2019 Binder free self-standing high performance supercapacitive electrode based on graphene/titanium carbide composite aerogel *Appl. Surf. Sci.* **481** 892–9

[61] Tu T, Liang B, Zhang S, Li T, Zhang B, Xu S, Mao X, Cai Y, Fang L and Ye X 2021 Controllable patterning of porous MXene (Ti_3C_2) by metal-assisted electro-gelation method *Adv. Funct. Mater.* **31** 2101374

[62] Yun T *et al* 2021 Multidimensional $Ti_3C_2T_x$ MXene architectures via interfacial electrochemical self-assembly *ACS Nano* **15** 10058–66

[63] Li L, Zhang M, Zhang X and Zhang Z 2017 New Ti_3C_2 aerogel as promising negative electrode materials for asymmetric supercapacitors *J. Power Sources* **364** 234–41

[64] Jiang Y, Xie X, Chen Y, Liu Y, Yang R and Sui G 2018 Hierarchically structured cellulose aerogels with interconnected MXene networks and their enhanced microwave absorption properties *J. Mater. Chem.* C **6** 8679–87

[65] Wang X, Fu Q, Wen J, Ma X, Zhu C, Zhang X and Qi D 2018 3D $Ti_3C_2T_x$ aerogels with enhanced surface area for high performance supercapacitors *Nanoscale* **10** 20828–35

[66] Guo J, Zhao Y, Liu A and Ma T 2019 Electrostatic self-assembly of 2D delaminated MXene (Ti_3C_2) onto Ni foam with superior electrochemical performance for supercapacitor *Electrochim. Acta* **305** 164–74

[67] Tian Y, Yang C, Que W, He Y, Liu X, Luo Y, Yin X and Kong L B 2017 Ni foam supported quasi-core-shell structure of ultrathin Ti_3C_2 nanosheets through electrostatic layer-by-layer self-assembly as high rate-performance electrodes of supercapacitors *J. Power Sources* **369** 78–86

[68] Tang Y, Yang C, Yang Y, Yin X, Que W and Zhu J 2019 Three dimensional hierarchical network structure of S-$NiFe_2O_4$ modified few-layer titanium carbides (MXene) flakes on nickel foam as a high efficient electrocatalyst for oxygen evolution *Electrochim. Acta* **296** 762–70

[69] Li X-P, Li Y, Li X, Song D, Min P, Hu C, Zhang H-B, Koratkar N and Yu Z-Z 2019 Highly sensitive, reliable and flexible piezoresistive pressure sensors featuring polyurethane sponge coated with MXene sheets *J. Colloid Interface Sci.* **542** 54–62

[70] Lin B *et al* 2020 MXene/chitosan nanocoating for flexible polyurethane foam towards remarkable fire hazards reductions *J. Hazard. Mater.* **381** 120952

[71] Zhao X, Zha X-J, Pu J-H, Bai L, Bao R-Y, Liu Z-Y, Yang M-B and Yang W 2019 Macroporous three-dimensional MXene architectures for highly efficient solar steam generation *J. Mater. Chem.* A **7** 10446–55

[72] Shi S, Qian B, Wu X, Sun H, Wang H, Zhang H-B, Yu Z-Z and Russell T P 2019 Self-assembly of MXene-surfactants at liquid-liquid interfaces: from structured liquids to 3D aerogels *Angew. Chem., Int. Ed. Engl.* **58** 18171–6

[73] Zhao M-Q, Xie X, Ren C E, Makaryan T, Anasori B, Wang G and Gogotsi Y 2017 Hollow MXene spheres and 3D macroporous MXene frameworks for Na-ion storage *Adv. Mater.* **29** 1702410

[74] Zhang X, Liu X, Dong S, Yang J and Liu Y 2019 Template-free synthesized 3D macroporous MXene with superior performance for supercapacitors *Appl. Mater. Today* **16** 315–21

[75] Song D, Li X, Li X-P, Jia X, Min P and Yu Z-Z 2019 Hollow-structured MXene-PDMS composites as flexible, wearable and highly bendable sensors with wide working range *J. Colloid Interface Sci.* **555** 751–8

[76] Bian R, Lin R, Wang G, Lu G, Zhi W, Xiang S, Wang T, Clegg P S, Cai D and Huang W 2018 3D assembly of Ti_3C_2-MXene directed by water/oil interfaces *Nanoscale* **10** 3621–5

[77] Yang Y, Wu L, Li L, Lin S, Bai L, Ma X, Shao Z and Zhang X 2020 Additive-free porous assemblies of Ti_3C_2T by freeze-drying for high performance supercapacitors *Chin. Chem. Lett.* **31** 1034–8

[78] Fan Z, Wang J, Kang H, Wang Y, Xie Z, Cheng Z and Liu Y 2020 A compact MXene film with folded structure for advanced supercapacitor electrode material *ACS Appl. Energy Mater.* **3** 1811–20

[79] Fan Z, Wang D, Yuan Y, Wang Y, Cheng Z, Liu Y and Xie Z 2020 A lightweight and conductive MXene/graphene hybrid foam for superior electromagnetic interference shielding *Chem. Eng. J.* **381** 122696

[80] Xu H, Yin X, Li X, Li M, Liang S, Zhang L and Cheng L 2019 Lightweight Ti_2CT_x MXene/poly(vinyl alcohol) composite foams for electromagnetic wave shielding with absorption-dominated feature *ACS Appl. Mater. Interfaces* **11** 10198–207

[81] Malik R 2018 Maxing out water desalination with MXenes *Joule* **2** 591–3

[82] Liu J, Zhang H-B, Xie X, Yang R, Liu Z, Liu Y and Yu Z-Z 2018 Multifunctional, superelastic, and lightweight MXene/polyimide aerogels *Small* **14** e1802479

[83] Lin P, Xie J, He Y, Lu X, Li W, Fang J, Yan S, Zhang L, Sheng X and Chen Y 2020 MXene aerogel-based phase change materials toward solar energy conversion *Sol. Energy Mater. Sol. Cells* **206** 110229

[84] Wang N-N *et al* 2019 Robust, lightweight, hydrophobic, and fire-retarded polyimide/MXene aerogels for effective oil/water separation *ACS Appl. Mater. Interfaces* **11** 40512–23

[85] Liang L, Li Q, Yan X, Feng Y, Wang Y, Zhang H-B, Zhou X, Liu C, Shen C and Xie X 2021 Multifunctional magnetic $Ti_3C_2T_x$ MXene/graphene aerogel with superior electromagnetic wave absorption performance *ACS Nano* **15** 6622–32

[86] Bayram V *et al* 2019 MXene tunable lamellae architectures for supercapacitor electrodes *ACS Appl. Energy Mater.* **3** 411–22

[87] Ran F, Wang T, Chen S, Liu Y and Shao L 2020 Constructing expanded ion transport channels in flexible MXene film for pseudocapacitive energy storage *Appl. Surf. Sci.* **511** 145627

[88] Fan Z, He H, Yu J, Liu L, Liu Y and Xie Z 2020 Lightweight three-dimensional cellular MXene film for superior energy storage and electromagnetic interference shielding *ACS Appl. Energy Mater.* **3** 8171–8

[89] Sun C, Shi X, Zhang Y, Liang J, Qu J and Lai C 2020 $Ti_3C_2T_x$ MXene interface layer driving ultra-stable lithium-iodine batteries with both high iodine content and mass loading *ACS Nano* **14** 1176–84

[90] Wang L, Qiu H, Song P, Zhang Y, Lu Y, Liang C, Kong J, Chen L and Gu J 2019 3D $Ti_3C_2T_x$ MXene/C hybrid foam/epoxy nanocomposites with superior electromagnetic interference shielding performances and robust mechanical properties *Composites* A **123** 293–300

[91] Chen Z, Hu Y, Zhuo H, Liu L, Jing S, Zhong L, Peng X and Sun R-C 2019 Compressible, elastic, and pressure-sensitive carbon aerogels derived from 2D titanium carbide nanosheets and bacterial cellulose for wearable sensors *Chem. Mater.* **31** 3301–12

[92] Li X *et al* 2020 3D-printed stretchable micro-supercapacitor with remarkable areal performance *Adv. Energy Mater.* **10** 1903794

[93] Gao C, Chen K, Wang Y, Zhao Y and Qu L 2020 2D graphene-based macroscopic assemblies for micro-supercapacitors *ChemSusChem* **13** 1255–74

[94] Yang P, Xia T, Ghosh S, Wang J, Rawson S D, Withers P J, Kinloch I A and Barg S 2021 Realization of 3D epoxy resin/$Ti_3C_2T_x$ MXene aerogel composites for low-voltage electrothermal heating *2D Mater.* **8** 025022

[95] Hu Y, Chen Z, Zhuo H, Zhong L, Peng X and Sun R-C 2019 Advanced compressible and elastic 3D monoliths beyond hydrogels *Adv. Funct. Mater.* **29** 1904472